CEBAF Program Advisory Committee Nine Proposal Cover Sheet

This proposal must be received by close of business on Thursday, December 1, 1994 at:

CEBAF
User Liaison Office, Mail Stop 12 B
12000 Jefferson Avenue
Newport News, VA 23606

Proposal Title

Study of the S_{11} (1535) Resonance Region via High Precision Eta Electro-Production Measurements

Contact Person

Name: W. Bertozzi or A. J. Sarty

Institution: Massachusetts Institute of Technology

Address: Laboratory for Nuclear Science, 26-441

Address: 77 Massachusetts Avenue

City, State ZIP/Country: Cambridge, MA 02139

Phone: (617) 253-7062 **FAX:** (617) 258-5440

E-Mail → Internet: bertozzi@mitlns.mit.edu or sarty@mitlns.mit.edu

Experimental Hall: A **Days Requested for Approval:** 22

Hall B proposals only, list any experiments and days for concurrent running:

CEBAF Use Only

Receipt Date: 12/15/94 PR 94-119

By: JP

BEAM REQUIREMENTS LIST

CEBAF Proposal No.: _____ Date: Dec. 14/94
(For CEBAF User Liaison Office use only.)

List all combinations of anticipated targets and beam conditions required to execute the experiment. (This list will form the primary basis for the Radiation Safety Assesment Document (RSAD) calculations that must be performed for each experiment.)

Condition #	Beam Energy (MeV)	Beam Current (μA)	Polarization and Other Special Requirements (e.g., time structure)	Target Material (use multiple rows for complex targets — e.g., w/windows)	Target Material Thickness (mg/cm²)
I(f)	4000	27	/	LH_2	1.062
I(b)	1600	27	/	LH_2	1.062
II	4000	27	/	LH_2	1.062
III	6000	27	/	LH_2	1.062
				WINDOWS: [redacted]	0.162
				Al	

The beam energies, E_{Beam}, available are: $E_{Beam} = N \times E_{Linac}$ where N = 1, 2, 3, 4, or 5. For 1995, E_{Linac} = 800 MeV, i.e., available E_{Beam} are 800, 1600, 2400, 3200, and 4000 MeV. Starting in 1996, in an evolutionary way (and not necessarily in the order given) the following additional values of E_{Linac} will become available: E_{Linac} = 400, 500, 600, 700, 900, 1000, 1100, and 1200 MeV. The sequence and timing of the available resultant energies, E_{Beam}, will be determined by physics priorities and technical capabilities.

HAZARD IDENTIFICATION CHECKLIST

CEBAF Proposal No.: _____ Date: Dec. 14/94
(For CEBAF User Liaison Office use only.)

Check all items for which there is an anticipated need.

Cryogenics
- _____ beamline magnets
- _____ analysis magnets
- ✓ target
  - type: LIQUID HYDROGEN
  - flow rate: 10 m/s (not critical)*
  - capacity: 20 ℓ

Electrical Equipment
- _____ cryo/electrical devices
- _____ capacitor banks
- _____ high voltage
- _____ exposed equipment

Radioactive/Hazardous Materials
List any radioactive or hazadorous/ toxic materials planned for use:
_____
_____
_____
_____

Pressure Vessels
- _____ inside diameter
- _____ operating pressure
- _____ window material
- _____ window thickness

Flammable Gas or Liquids
- type: LIQUID HYDROGEN
- flow rate: 10 m/s
- capacity: 20 ℓ

Drift Chambers
- type: STANDARD HALL A VDC
- flow rate: _____
- capacity: _____

Other Target Materials
- ___ Beryllium (Be)
- ___ Lithium (Li)
- ___ Mercury (Hg)
- ___ Lead (Pb)
- ___ Tungsten (W)
- ___ Uranium (U)
- ___ Other (list below)

_____
_____

Vacuum Vessels
- _____ inside diameter
- _____ operating pressure
- _____ window material
- _____ window thickness

Radioactive Sources
- _____ permanent installation
- _____ temporary use
- type: _____
- strength: _____

Large Mech. Structure/System
- _____ lifting devices
- _____ motion controllers
- _____ scaffolding or
- _____ elevated platforms

Lasers
- type: _____
- wattage: _____
- class: _____

Installation:
- _____ permanent
- _____ temporary

Use:
- _____ calibration
- _____ alignment

Hazardous Materials
- ___ cyanide plating materials
- ___ scintillation oil (from)
- ___ PCBs
- ___ methane
- ___ TMAE
- ___ TEA
- ___ photographic developers
- ___ other (list below)

_____
_____

General:

Experiment Class:

- _____ Base Equipment
- _____ Temp. Mod. to Base Equip.
- _____ Permanent Mod. to Base Equipment
- _____ Major New Apparatus

Other: _____
_____

LAB RESOURCES REQUIREMENTS LIST

CEBAF Proposal No.: _____ Date: DEC. 14/94
(For CEBAF User Liaison Office use only.)

List below significant resources — both equipment and human — that you are requesting *from CEBAF* in support of mounting and executing the proposed experiment. Do not include items that will be routinely supplied to all running experiments, such as the base equipment for the hall and technical support for routine operation, installation, and maintenance.

Major Installations *(either your equip. or new equip. requested from CEBAF)*

STANDARD

New Support Structures: /

Data Acquisition/Reduction

Computing Resources: STANDARD

New Software: /

Major Equipment

Magnets: STANDARD

Power Supplies

Targets

Detectors

Electronics

Computer Hardware

Other

Other

PROPOSAL TO THE CEBAF PAC9

Study of the $S_{11}(1535)$ Resonance Region via High Precision Eta Electro-Production Measurements

Spokespersons:

A. Afanas'ev (Kharkov & CEBAF), W. Bertozzi (MIT),

S. Gilad (MIT), A.J. Sarty (MIT)

Contact Persons:

W. Bertozzi and A.J. Sarty

HALL A COLLABORATION PROPOSAL

List of Institutions:

Massachusetts Institute of Technology, Cambridge, MA
Continuous Electron Beam Accelerator Facility, Newport News, VA
Kharkov Institute of Physics and Technology, Kharkov, UKRAINE
Universität Bonn, Bonn, GERMANY
California State University, Los Angeles, CA
Chungnam National University, Taejon, KOREA
George Washington University, Washington, DC
University of Georgia, Athens, GA
INFN Sezione di Bari, Bari, ITALY
INFN Sezione Sanita, Rome, ITALY
Kent State University, Kent, OH
University of Kentucky, Lexington, KY
University of Maryland, College Park, MD
Old Dominion University, Norfolk, VA
University of Regina, Regina, CANADA
Rutgers University, Piscataway, NJ
University of Virgina, Charlottesville, VA
College of William and Mary, Williamsburg, VA
Yerevan Physics Institute, Yerevan, ARMENIA

Date	Description	TotaL Hours	Energies	Luminosity
Dec. 15, 1994	p(e,e′p)η	528	1.6, 4.0, 6.0 GeV	$1.1 \times 10^{38} s^{-1} cm^{-2}$

LIST OF PARTICIPANTS

W. Bertozzi, S. Gilad, A.J. Sarty, J. Zhao*
Massachusetts Institute of Technology
J.-P. Chen, J. Gomez, J. LeRose, R. Michaels, S. Nanda, A. Saha, B. Wojtsekhowski
Continuous Electron Beam Accelerator Facility
A. Afanas'ev*†, A. Glamazdin, V. Gorbenko, P. Sorokin
Kharkov Institute of Physics and Technology
R. Gothe*
Universität Bonn
M. Epstein
California State University
J.-C. Yang*
Chungnam National University
B. Briscoe*, T.W. Morrison*, Z. Papandreou, S. Philips*, J. Prokip*
George Washington University
P. Rutt
University of Georgia
R. De Leo
Universit di Bari and INFN Sezione di Bari
E. Cisbani, S. Frullani, F. Garibaldi, M. Jodice, G.M. Urciuoli
Istituto Superiore di Sanita and INFN Sezione Sanita
D.M. Manley
Kent State University
D.S. Dale, B.C. Doyle*
University of Kentucky
C.C. Chang, J.J. Kelly, P. Markowitz, T. Payerle*
University of Maryland
P. Ulmer, L. Weinstein
Old Dominion Univeristy
G. Huber, G. Lolos
University of Regina
E. Brash, R. Gilman, C. Glashausser, G. Kumbartzki, R. Ransome
Rutgers University
H. Baghaei, R.W. Lourie
University of Virgina
J.M. Finn, M. Jones, C. Perdrisat
College of William and Mary
A. Gasparian, H. Voskanian
Yerevan Physics Institute

and the rest of the Hall A Collaboration

*: *Not Hall A Collaboration Members*
†: *Permanent address: CEBAF, Newport News, VA*

ABSTRACT

We propose to measure the p(e,e′p)η reaction in the region near-threshold. The purpose of these proposed measurements is to obtain high precision, accurate data in the region near threshold. These data will allow a multipole analysis which will adequately constrain models of the eta electro-production process, which is dominated by the excitation of the $S_{11}(1535)$ resonance. The $S_{11}(1535)$ is interesting from the points of view that it has an anomalously flat form-factor, and is the only resonance in this energy region with any appreciable coupling to the ηN channel. However, the possibility of contributions from the $P_{11}(1440)$ and $D_{13}(1520)$ resonances, as well as s-, p-, and d-wave non-resonant Born terms, also exists. Present data do not allow separation of any of these small contributions. We propose to obtain full eta angular distributions in the center-of-mass system, as a function of excitation energy up to approximately 20 MeV above threshold, with very good energy and angular resolutions, and very good statistical precision. Measurements will be made at Q^2 values of 3.0 and 4.0 $(GeV/c)^2$, and at a Q^2 of 0.65 $(GeV/c)^2$ where we will also perform a Rosenbluth separation to individually determine the longitudinal and transverse contributions for the first 4 MeV above threshold. These measurements will provide accurate data of the angular distributions as a function of energy to allow separation of any small contributions to the form-factor from the non-dominant terms. Thus, it will provide new information on the $S_{11}(1535)$ with unprecedented energy resolution. By staying at energies near the eta-production threshold (up to approximately +20 MeV), we will exploit the fact that the emitted protons are "kinematically focused" along the direction of the momentum transfer vector, thus allowing full use of the high resolution capabilities of the HRS spectrometers in Hall A.

1. Introduction

The study of nucleon resonances is an important tool for furthering our understanding of quark models of the nucleon. Accordingly, a rich program to study nucleon resonances is planned and approved for CEBAF. In particular, the electro-magnetic coupling to the resonances can be calculated with relatively small model dependence, once the baryon wave-functions are known [Fos 83]. Hence, the study of these couplings is a useful tool in constraining quark models of the nucleon. In electroproduction, it is possible to measure the form-factor of resonances, as well as the nature of their excitation. The latter can be characterized by multipole decomposition, and by the responses to the longitudinal and transverse states of the virtual photons.

This proposal is primarily aimed at studying the $S_{11}(1535)$ nucleon resonance via the electroproduction of etas. Electro-eta production is a powerful tool in the study of the $S_{11}(1535)$ and its electromagnetic couplings. In the energy range of up to 2 GeV only the $S_{11}(1535)$ has a significant decay branching-ratio, ~50%, to ηN [Par 94]. Hence, the existence of an eta in the final state can, to a large extent, provide a tag to the excitation of this resonance, thus enabling its separation from overlapping neighboring resonances. Therefore, the study of the $S_{11}(1535)$ can be done very cleanly through the electro- and photoproduction of etas. Nevertheless, the existence of an eta in the final state does not exclude completely contribution from competing processes, such as the excitation of neighboring resonances whose decay branching ratios to ηN are very small but not zero, or the non-resonant Born terms. To separate these contributions, additional tools can be used, such as multipole decomposition of the excitation, and the energy dependence of these contributing multipoles. In the case of the $S_{11}(1535)$, the competing processes which contribute to the measured ηN final state are the Born terms, and the excitations of the overlapping $P_{11}(1440)$ and $D_{13}(1520)$ resonances, whose decay branching ratios to ηN are on the order of 1%. Study of the Born terms is in itself interesting, since it provides a valuable handle to the determination of the relatively weak and poorly known ηNN coupling [Tia 94]. Knowledge of the ηNN (and $\eta' NN$) coupling constants has fundamental meaning, and can provide, for example, access to the problem of the fraction of nucleon spin carried by quarks [Hat 90, Efr 90, Dor 90].

We propose to perform precision measurements of the angular distributions of electro-eta production from threshold to approximately 20 MeV above it. These measurements will be done at two transferred momenta, $Q^2 = 2.0$ and 3.0 $(GeV/c)^2$, and will provide the distribution of etas in both θ and ϕ in the center-of-mass system. The angular distributions will enable an angular momentum and multipole decomposition and hence, separate contributions from the $P_{11}(1440)$ and $D_{13}(1520)$ resonances. The dependence of the different multipole strengths on the excitation energy, will allow the separation of the resonances from the Born terms, since the latter are expected to have much weaker energy dependence. As mentioned, the Born terms are interesting due to their relation to the ηNN coupling and hence should not be viewed only as "background". Finally, the measurements at the two Q^2 values will facilitate the determination of the $S_{11}(1535)$ form

factor. In addition, at a lower momentum transfer, $Q^2 = 0.65$ (GeV/c)^2, we propose to perform a Rosenbluth separation near the eta-production threshold. This low Q^2 measurement also will yield another point for the form-factor near threshold. All these measurements take advantage of (and are limited by) the unique capabilities of Hall A, and are complementary to those approved for CLAS. In particular, we take advantage of the "kinematic focusing" which occurs near the eta-production threshold, and the high resolution spectrometers of Hall A. Obviously, the relatively small acceptance of these spectrometers imposes a limit to the range of accessible excitation energy. This limitation, however, is compensated by the very good resolution which can be obtained for the excitation energy, $\delta W \simeq 1$ MeV (FWHM).

Other unique capabilities of Hall A will be utilized in the future, when we intend to measure transferred and induced polarization observables in the excitations of these three resonances and the non-resonant Born terms. The technique of using the kinematic focusing, combined with the high resolution spectrometers in Hall A, can be similarly used to study the isospin dependence of the eta-production process, by measuring coherent eta production on deuterium, ^{3}He and ^{4}He. Finally, the same capabilities of Hall A can extend these studies to other resonances which decay into a nucleon and one other meson (such as η'N). Such issues are now under study by our group, and will be the subject of future proposals.

2. Background and Motivation

The threshold for eta production from the proton is defined by an invariant mass of the final ηp state, W, of 1485.7 MeV. Earlier measurements have established that electro- and photoproduction of etas are dominated by resonance excitation [Baj 69, Bec 74, Ald 75, Bra 84, TAPS 94]. This may be understood in terms of the facts that the η is a neutral meson, and that the ηNN coupling constant is weak [Tia 94, and references therein], both of which conspire to reduce the contribution from the "background" Born terms. However, electro-and photo-production of etas can proceed via the excitation of only selected resonances since the eta, an isoscalar, can couple only to resonances with T = ½. Moreover, the fact that the decay branching ratio to ηN is small to all but the $S_{11}(1535)$ in the energy region up to 2 GeV, makes this process even more selective.

Electro- and photo-production of etas in the region of the $S_{11}(1535)$ resonance have been studied experimentally between 1973 and 1984 [Baj 69, Kum 73, Bec 74, Ald 75, Bra 84]. New experiments are being performed at Mainz [TAPS 94] and Bonn [Wil 93]. The cross-section for the excitation of the $S_{11}(1535)$ resonance rises fast with energy and peaks at W=1535 MeV. The proximity of the eta-production threshold to the peak of the resonance, and the strong coupling of the resonance to the ηN channel, indicate that the resonance excitation dominates, and that non-resonant background terms must be small. Indeed, earlier analyses of photo -and electro-production of etas in the $S_{11}(1535)$ region have attributed almost the entire cross-section to the excitation of the resonance [for

example, Baj 69, Ald 75, Bra 84]. This has been confirmed by preliminary results of the recent eta-photoproduction measurement in the $S_{11}(1535)$ region at MAMI [TAPS 94]. In fact, the isotropic angular distributions in the earlier measurements have established that the excitation in the region of the $S_{11}(1535)$ proceeds almost entirely via an s-wave [Bra 84]. Hence, interpretation of the earlier data was based on the assumption that the entire resonant excitation of the cross-section is due to an s-wave transition. Two of the earlier DESY and BONN electroproduction experiments have separated the longitudinal and transverse responses [Bra 78, Bre 78]. The precision which was achieved in these measurements could only establish that in the energy range of 1.49-1.58 GeV, the ratio $R=\sigma_L/\sigma_T$ is 0.23 ± 0.11, 0.22 ± 0.23 and -0.16 ± 0.16 respectively for $Q^2 = 0.4$, 0.6 and 1.0 $(GeV/c)^2$.

From the available data, the $S_{11}(1535)$ resonance stands out as having several unique features:

- The $S_{11}(1535)$ is the only N^* resonance with a large, ~ 50%, decay branching ratio to ηN. All the neighbouring resonances, including the $S_{11}(1650)$, have very small decay branching ratios to this channel.
- Assuming that the entire eta-production cross-section is due to the excitation of the $S_{11}(1535)$, the measured cross-section falls off anomalously slowly with the transferred momentum [Bra 84]. This is shown in Figure 1, which is taken from Reference [Bra 84]. While the nearby $D_{13}(1520)$ falls off as an exponential to the power 1.60 ± 0.06, the S_{11} falls off as an exponential to the power 0.386 ± 0.013. This feature is not only unique, but is especially surprising considering that the $D_{13}(1520)$, which displays the much sharper but common cross-section fall-off with Q^2, is a member of the same SU(6) octet and is a symmetry partner of the $S_{11}(1535)$ in Constituent Quark Models [Kon 80].

These features are not adequately and consistently explained by theoretical models of the nucleon [for example, Figure 9 in Ald 75, and Figure 1 in CLAS 89]. It was suggested [Bra 78, Bre 78] that the anomalously flat form-factor of the $S_{11}(1535)$ arises from large longitudinal contributions to the cross-section. However, these suggestions are not substantiated by the relatively small longitudinal contribution extracted from the data. Recent calculations by Konen and Weber [Kon 90] suggest that Relativistic Quark Models (RQM) naturally give rise to large longitudinal contributions to the $S_{11}(1535)$ form-factor which may explain the flat form-factor. Again, this cannot be substantiated by the existing data, which is also not good enough to distinguish between widely varying predictions of the longitudinal component [Kon 90]. In fact, Konen and Weber specifically indicate the need for precise measurements of σ_L at $Q^2 < 1$ $(GeV/c)^2$ in order to check various RQM models.

The availability of modern facilities, as well as the continuous interest in the understanding of the electro- and photoproduction of the $S_{11}(1535)$ resonance, have given rise

to a new generation of experiments. Preliminary data from MAMI indicate that eta photoproduction in the $S_{11}(1535)$ region occurs almost entirely by resonance excitation. Although these high-resolution data are of high quality, the use of real photons prevents the measurement of the longitudinal response, nor does it allow the study of the Q^2 dependence of the cross section. An effort is underway at Bonn to measure eta electroproduction in the $S_{11}(1535)$ resonance region [Got 94]. These measurements will utilize a large time-of-flight detector wall to measure the angular distributions of the outgoing proton. The facility at Bonn lends itself to multipole decomposition and the determination of the LT (σ_{LT}) and TT (σ_{TT}) interference responses, as well as to the measurement of the Q^2 dependence of the cross section. However, the excitation energy (W) resolution of the data will not be as good as is possible in Hall A (FWHM $\leq$ 5 MeV), and the Bonn measurements will focus on the $Q^2 \leq 1.5$ $(GeV/c)^2$ region [Got 94]. An experiment is approved for CLAS [CLAS 89], which will measure the electroproduction of etas in a wide excitation energy range. Here, a multipole decomposition will be obtained over a Q^2 range of 0.2-4.0 $(GeV/c)^2$, and the determination of σ_{LT} and σ_{TT} is possible, but the resolution in W of these data is expected to be about 20 MeV. In addition, CLAS does not facilitate good measurement of the longitudinal response via Rosenbluth separation.

Clearly, for a complete understanding of the $S_{11}(1535)$, better data are needed to separate the small resonant contributions of the $P_{11}(1440)$ and $D_{13}(1520)$ from the $S_{11}(1535)$. Not only will this separation clarify the situation for the $S_{11}(1535)$, but any evidence of contributions from the other two resonances will be important since there is no experimental data showing their coupling to the eta. It is also important to separate out the non-resonant contributions to the L=0 partial wave of the reaction [Tia 94]. Finally, a more precise determination of the longitudinal response is needed [Kon 90]. With these multifaceted data available, a better determination of the $S_{11}(1535)$ form-factors and the electromagnetic couplings will be possible. This experiment will provide high resolution data in energy (W), and in both center-of-mass angles, θ and ϕ, of the eta from threshold to approximately 20 MeV above it. It will allow high quality decomposition of the contributing multipoles, and separation of the Born from the resonant terms. A detailed multipole analysis of eta photoproduction from nucleons has been done by [Tia 94] and [Ben 94]; our experiment will provide data to extend such analyses to the case of virtual photons. The measurement at $Q^2 = 3.0$ and 4.0 $(GeV/c)^2$, will provide a clean measure of the form-factor, and the one at $Q^2 = 0.65$ $(GeV/c)^2$ will also allow good separation of its longitudinal and transverse components near threshold. In addition, the data obtained on the Born terms, can provide significant information towards the understanding of the fundamental ηNN coupling. As such, this experiment is complementary to the approved CLAS experiment, which will cover a larger W range, but cannot probe the kinematic range that we propose in the detail and precision that this experiment will allow.

It was already mentioned that the technique we propose, utilizing the kinematic focusing together with the capabilities of Hall A, provides natural future extensions to this experiment. The availability of polarized beam and a hadron polarimeter in Hall A will allow the study of polarization observables in the $p(\vec{e},e'\vec{p})\eta$ reaction. The polarization of the emitted proton is an effective probe of the interference terms between different multipole transitions. This property of polarization observables will be used in an approved CEBAF experiment, PR-91-011 (Co-Spokesmen: S.Frullani and R.Lourie), to study the electro-excitation form factors of the Delta and Roper resonances. The value of polarization observables in pion electroproduction from the nucleon has already received recognition [e.g., Dom 69, Ras 89]. The same arguments can be applied to eta electroproduction. For example, the in-plane longitudinal and transverse components of the recoil-proton polarization in the $S_{11}(1535)$ resonance region can be measured, and will allow the extraction of the ratio of scalar to transverse transition form-factors, $S_{1/2}/A_{1/2}$, in a manner whereby a number of systematic errors cancel. The formalism for the polarization observables (and also the unpolarized observables to be directly addressed by the experiment proposed here), and the contribution to the various terms from the different multipoles, is given in Reference [Ras 89]. Further study is ongoing to determine optimum experimental configurations to access these polarized observables.

3. Phenomenology

The inelastic electron scattering cross section can be factorized into the product of a "virtual photon flux factor", Γ_t, and the virtual photon absorption cross section, σ_v [Fos 83]. For the particular case of final states consisting of a single η meson and a nucleon, we can define a polar coordinate system $(\theta_\eta^*, \phi_\eta^*)$ for the η in the ηN center-of-mass system (CMS), with the z-axis oriented along the direction of the virtual photon momentum vector ($\vec{q}$). Then, the differential cross section may be written:

$$\frac{d^3\sigma}{d\omega\, d\Omega_e\, d\Omega_\eta^*} = \Gamma_t \times \frac{d\sigma_v}{d\Omega_\eta^*}(W,Q^2) \quad ; \qquad (1)$$

with the following definitions for kinematic variables which are used throughout the proposal:

$$\begin{aligned}
\Gamma_t &= \frac{\alpha}{2\pi^2} \cdot \frac{E_e'}{E_o} \cdot \frac{W^2 - m_p^2}{2m_pQ^2} \cdot \frac{1}{1-\varepsilon} \\
W &= (m_p^2 + 2m_p\omega - Q^2)^{1/2} \\
Q^2 &= \vec{q}^2 - \omega^2 \qquad (2) \\
\varepsilon &= \left[1 + 2\frac{\vec{q}^2}{Q^2}\tan^2\left(\frac{\theta_e}{2}\right)\right]^{-1} ,
\end{aligned}$$

where ω and $\vec{q}$ are the energy and momentum (in the lab) transferred by the virtual photon, respectively. Also, relevant for later discussions, is the excitation energy above the η-production threshold:

$$\Delta W \equiv W - W_{thresh} = W - (m_p + m_\eta) \qquad (3)$$

In the One Photon Exchange Approximation, assuming an unpolarized incident electron beam and an unpolarized target, the virtual photon absorption cross section can be separated into the longitudinal (L), transverse (T), and LT- and TT- interference responses:

$$\frac{d\sigma_v}{d\Omega_\eta^*} = \frac{d\sigma_T}{d\Omega_\eta^*} + \varepsilon \frac{d\sigma_L}{d\Omega_\eta^*} + \varepsilon \cos(2\phi_\eta) \frac{d\sigma_{TT}}{d\Omega_\eta^*}(\sin^2\theta_\eta^*) \qquad (4)$$

$$+ \sqrt{2\varepsilon(\varepsilon+1)} \cos(\phi_\eta) \frac{d\sigma_{LT}}{d\Omega_\eta^*}(\sin\theta_\eta^*) \ .$$

The angle $\phi_\eta = \phi_\eta^*$ is measured in the lab between the electron scattering plane (which contains the incoming and scattered electrons) and the so-called reaction plane (which contains $\vec{q}$ and the outgoing eta momentum vector). Since the photon flux-factor (Γ_t) and the degree of virtual photon polarization (ε) both depend solely on the electron kinematics, all information on the electromagnetic transition current to the ηN state is contained in the σ_v responses.

Each of σ_{LT}, σ_{TT}, and $(\sigma_T + \varepsilon\,\sigma_L)$, have unique dependencies on $\cos\theta_\eta^*$, with the strength distribution determined by the specific partial waves contributing to each term. In addition, σ_{LT} has an explicit dependence on $\sin\theta_\eta^*$, and σ_{TT} on $\sin^2\theta_\eta^*$. Specifically, if only the first 3 leading order partial waves are considered (L = 0,1, and 2), and assuming that the L=0 s-wave part is dominant over the other partial wave contributions, then the following statements regarding the angular distributions can be made. The σ_{TT} part, with an azimuthal $\cos2\phi_\eta$ dependence, has only a $\sin^2\theta_\eta^*$ polar dependence with the strength determined by the partial-wave interference between the dominant s-wave and the smaller d-wave. The σ_{LT} part has an $\cos\phi_\eta$ azimuthal dependence, which is multiplied by two polar angular-dependence terms: *(i)* a $\sin\theta_\eta^*$ term with the amplitude coming from the interference of the dominant s-wave with any p-wave component, and *(ii)* a $\sin\theta_\eta^*\cos\theta_\eta^*$ term arising from the interference of the s-wave with the d-wave. The azimuthally independent parts, σ_L and σ_T, have isotropic components driven by the dominant s-wave with a small contribution from the interference of the s- and d-waves, as well as having on both $\cos\theta_\eta^*$ (from s-p interference) and $\cos^2\theta_\eta^*$ (from s-d interference). More specific details on the manner in which the various s-, p-, and d- partial waves contribute to the various terms can be found in References [Ras 89] and [Wil 93].

From the equations [(1) and (4)] and discussion above, it is clear that measurements which map the full ϕ_η distribution will allow separation of the LT and TT interference responses for specific values of W and Q^2, while mapping the full $\cos\theta_\eta^*$ range enables a

multipole decomposition. It should be noted that, if absolutely no contributions from p- or d-wave are present (i.e. only the s-wave ηN multipole), then the LT and TT responses are both identically zero. As will be shown in the upcoming sections, the statistical and relative systematic precision with which we will obtain for the angular distributions will allow measurements of both σ_{TT} and σ_{LT} even if they are as small as a few percent of the total cross section. The individual L and T responses can be determined via a usual Rosenbluth-type separation by measuring the cross section at a fixed (W,Q^2) point with two values of ε. We will obtain sufficient statistical precision to extract the ratio of $R = \sigma_L/\sigma_T$ to an absolute level of $\simeq \pm 0.03$ (with a systematic uncertainty on the same order).

4. Kinematics

The specific choices of kinematical setups proposed here were primarily driven by three factors:

i. the higher the momentum transfer we can access, the more kinematically focused the protons are along $\vec{q}$, and thus the larger the range in ΔW for which we obtain the full 4π in $\Delta\Omega_\eta^*$;

ii. a relatively big spread in Q^2 values is desired for determination of the form-factor dependence;

iii. a large spread in ε is needed between the forward and backward electron-angle measurements in order to facilitate as good a Rosenbluth separation as possible.

In line with these factors, the following 3 electron kinematics were chosen:

- **KIN I** $Q^2 = 0.65$ (GeV/c)^2 → for σ_L, σ_T separation
  Forward Angle - KIN I(f): $E_o = 4.0$ GeV ($\varepsilon = 0.93$)
  Backward Angle - KIN I(b): $E_o = 1.6$ GeV ($\varepsilon = 0.44$)
- **KIN II** $Q^2 = 3.0$ (GeV/c)^2
  $E_o = 4.0$ GeV
- **KIN III** $Q^2 = 4.0$ (GeV/c)^2
  $E_o = 6.0$ GeV

These 3 kinematics are shown graphically in Figure 2. This figure shows the kinematic contours for p(e,e′p)η at ΔW=0 (threshold) plotted in the space of electron scattering angle versus the angle of $\vec{q}$. Curves are shown for the three proposed beam energies (1.6, 4.0, and 6.0 GeV). The low Q^2 point, KIN I, is seen to be a good choice for yielding a large "lever arm" for the Rosenbluth separation ($\varepsilon_{for} = 0.93$, and $\varepsilon_{back} = 0.44$). The higher Q^2 points (KIN II and III) give the largest ΔW coverage consistent with reasonable counting rates and, together with KIN I, span a broad momentum transfer range for form-factor determination.

We take advantage of the "kinematic focusing" in detecting the protons from the reaction p(e,e′p)η. To demonstrate the effect of kinematic focusing, Figure 3 shows how the cone of emitted protons from p(e,e′p)η opens up around $\vec{q}$ as ΔW increases. In this figure, the solid lines show how, at a fixed value of ΔW, the proton momentum and angle with respect to $\vec{q}$ (θ_{pq}) vary over the whole decay-cone of the η ($\theta_\eta^* = 0° \rightarrow 180°$). It can be seen that for KIN II, at 16 MeV above threshold, the maximum angular deviation of the protons from the $\vec{q}$ direction is less than 3.5°.

TABLE 1. Central Kinematic Values for Proposed Measurements

KIN		Q^2	E_o	ELECTRON ARM				PROTON ARM	
		$(GeV/c)^2$	(GeV)	θ_e (°)	ω (MeV)	ΔW (MeV)	θ_q (°)	P_p (MeV/c)	θ_p (°)
I(f)	#1	0.65	4.0	13.49	1056.7	2.0	-31.11	761.9	-32.83
	#2							838.9	
	#3							921.1	
	#4							921.1	-29.39
	#5							838.9	
	#6							761.9	
I(b)	#1	0.65	1.6	51.24	1056.7	2.0	-18.48	761.9	-20.20
	#2							838.9	
	#3							921.1	
	#4							921.1	-16.76
	#5							838.9	
	#6							761.9	
II	#1	3.0	4.0	39.01	2317.8	7.5	-21.46	1657.1	-23.18
	#2							1823.5	
	#3							2004.2	
	#4							2004.2	-19.74
	#5							1823.5	
	#6							1657.1	
III	#1	4.0	6.0	26.62	2854.7	10.0	-23.85	1990.5	-25.57
	#2							2195.1	
	#3							2421.0	
	#4							2421.0	-22.13
	#5							2195.1	
	#6							1990.5	

For each electron kinematic setting, six proton spectrometer settings will be used. These 6 proton settings are placed symmetrically in (P_p, θ_p) about the central momentum transfer direction. In this way, by measuring for an equal time at each setting, the most

efficient coverage of the ηp decay-cone can be obtained for a given ΔW range. Table 1 details the spectrometer settings to be used for each of the kinematic points. Details of the acceptances as a function of ΔW for each kinematic point are given in the next section.

5. Measurement Details: Resolutions, Acceptances, and Count-Rates

5.1 Monte Carlo Simulations

In order to evaluate experimental details such as resolution, count-rates over finite acceptances, etc., a computer Monte Carlo code was developed ("ETA_ACC"). This code is similar in nature to the code MCEEP [Ulm 91], except that it is less general (e.g. spectrometer transport matrix analysis is not incorporated) and specifically written at this time for the p(e,e′p)η reaction. The code ETA_ACC accounts for the finite acceptances and resolutions in both spectrometers, and can sample either from phase-space distributions (to examine acceptance volumes) or from cross-section-weighted distributions (for count-rate estimates).

To make estimates regarding expected p(e,e′p)η count-rates, we used a cross-section parameterization of the existing data. The prescription used is as follows. Firstly, since as discussed thoroughly in the preceding sections, existing data are consistent (within the acquired precision) with s-wave distributions only, the η's are generated isotropically in the ηp CMS. Secondly, since the Monte Carlo generates, for every excitation energy W sampled, the full 4π angular distributions in the ηp CMS, the relevant cross section weightings need not be differential in $d\Omega_\eta^*$:

$$\frac{d^2\sigma}{d\omega d\Omega_e} = \Gamma_t \times \sigma_v(W,Q^2) \quad . \tag{5}$$

The W-dependence used for σ_v was a relativistic Breit-Wigner function for the $S_{11}(1535)$, as parametrized and fitted to data in Reference [Bre 78]. To get an appropriate Q^2 dependence, the absolute value of the Breit-Wigner fit from [Bre 78] (which was measured at $Q^2 = 0.4$ (GeV/c)^2) was scaled by the logarithmic decrease as shown in Figure 1 (from [Bra 84]). Such a parameterization for $\sigma_v(W,Q^2)$, along with the appropriate Mott-type cross-section variation of Γ_t , gives a reasonable estimation of the expected p(e,e′p)η counting rates.

5.2 Resolutions

In order to understand to what degree various kinematical variables such as the missing mass (M_{miss}), θ_η^*, ϕ_η, and W can be resolved, our Monte Carlo code was used to "smear" the spectrometer variables by their expected resolution functions. For the electron spectrometer, angular resolutions slightly worse than the design goal values [CDR 90, see page A4-29] were assumed: $\delta\phi_e^{transport} = 0.59$ mr (FWHM), and $\delta\theta_e^{transport} = 1.18$ mr (FWHM). These resolution values include the effects of multiple scattering in the

spectrometer windows, VDC's, etc. Additional angular smearing due to multiple scattering of the electrons in the target and target walls will be small owing to the high energy of the electrons and the thin target to be used, thus the resolution values used in our simulation should adequately account for these effects. Since the multiple scattering of the protons will be a larger effect, the angular resolutions we assume for the proton spectrometer were: $\delta\phi_p^{transport}$ = 1.00 mr (FWHM), and $\delta\theta_p^{transport}$ = 2.35 mr (FWHM). The momentum resolutions we applied were more relaxed compared to the design goal: $\delta P_e/P_e = \delta P_p/P_p = 3 \times 10^{-4}$ (design goal = 1×10^{-4}).

Using the values quoted above, we determined the FWHM resolution in W to be $\lesssim$ 0.7 MeV for KIN I, $\lesssim$ 0.9 MeV for KIN II, and $\simeq$ 2.0 MeV for KIN III. The missing mass resolution is equally good, ranging from 1.0-1.5 MeV (FWHM) for KIN I and II, and 3.0-3.5 for KIN III. Finally, the resolution for the reconstruction of CMS η angles are (FWHM): $\delta\theta_\eta^* < 5°$, and $\delta\phi_\eta < 10°$.

The W-resolution quoted above is calculated using only electron-arm coordinates. However, it should be noted that it will be possible to use the proton coordinates to help tighten up the W-resolution. This can be understood with reference to Figure 3: for a particular W-value, there is a specific range of the proton cone both in momentum and angle. Examination of these ranges gives additional information on the limits of W accepted. It can be added here that this aspect of using the proton-cone range is very useful in terms of self-calibrating the experiment as a whole. For example, any offsets in the incident beam energy or electron scattering angle, are manifested either in shifts of the missing mass peak (away from the η-mass value of 547.45 MeV), or of the expected proton cone range for a particular W-range.

However, the most sensitive tool we will have for self-calibrating the experiment is the existence of a threshold and the dramatic increase in the cross section as a function of ΔW near the η-threshold. Given the W-resolution of 0.7 MeV (FWHM) for the forward angle measurement in KIN I, shifts in ΔW of roughly 0.1 MeV or less will be detectable. For KIN I(f), this would correspond to about a 0.5×10^{-4} relative shift in E_o. Thus, the absolute scale of ΔW (which is defined as the amount of energy *above threshold*) will be known to this level of precision.

5.3 Count Rates and Acceptances

All of the count-rate calculations were performed assuming that we will use the standard Hall A 15 cm long liquid hydrogen target, and 27 μAmps of beam current. This results in a luminosity of 1.1×10^{38} $s^{-1}cm^{-2}$. These conditions require less than 100 Watts of cooling power for the target. A cryogenic target system is already planned for Hall A which will be capable of much higher cooling power, and is in fact a requirement for several already approved Hall A Collaboration experiments. As such, our luminosity assumption should be reasonably obtained with the standard Hall A equipment. It should be noted that we have no restrictions against using a shorter target, and compensatory higher beam current (e.g. a 4 cm long target, with 100 μAmps), as long as we achieve the

same luminosity.

The momentum acceptance of both spectrometers was assumed to be ±5% of the central momentum value. For all proton spectrometer settings, the full angular acceptance was assumed, $\Delta\Omega$ = 7.8 msr. The angular acceptance used for the electron spectrometer varied depending on the particular kinematics; details of this are given below.

The region of phase space covered by the spectrometers for this measurement is demonstrated in Figure 4. This figure shows simulation results for KIN II. Shown are the regions populated for a ΔW range of 0-15 MeV. The location of the 6 proton spectrometer settings are shown in the middle and bottom graphs by the solid lines. Note that, in these graphs, the origin of the proton spectrometer transport-angle system ($\phi_p^{transport}$, $\theta_p^{transport}$) is located directly along the central $\vec{q}$ direction (θ_q = -21.46°).

For KIN II and for KIN I(b), we can utilize the full angular acceptance of the electron spectrometer: $\Delta\phi_e^{transport} = \pm$ 30 mr, and $\Delta\theta_e^{transport} = \pm$ 60 mr. However, for the other 2 kinematics, I(f) and III, it is necessary to restrict the angular acceptance of the electron for analysis of p(e,e′p)η events. This need can be understood with reference to the top graph in Figure 4; this graph shows the correlation between electron angle and momentum required to obtain a certain value of W. Because of this correlation, when examining a small ΔW bin, as the electron angle varies so too does the electron momentum. These variations show themselves as a displacement of the proton cone from p(e,e′p)η, both in proton angle and momentum. Given the limited region of proton angle and momentum which can be easily accessed with as few different spectrometer settings as possible (shown as the 6 proton settings in Figure 4), accepting a too large electron-angle range can result in moving the proton cone outside of the accepted region. For this reason, the usable electron acceptance is limited to: $\Delta\phi_e^{transport} = \pm$ 10 mr, $\Delta\theta_e^{transport} = \pm$ 10 mr for KIN I(f); and $\Delta\phi_e^{transport} = \pm$ 30 mr, $\Delta\theta_e^{transport} = \pm$ 30 mr for KIN III. These angular restrictions may be done in software during data analysis, or could be done using custom collimators in order to reduce singles rates in the electron spectrometer (although these singles rates are not prohibitively high, as will be shown in the next section). All rate estimates and quoted run times account for these restricted acceptances.

In order to acquire sufficient statistics to enable binning in both θ_η^* and ϕ_η^*, 25 hours of running time at each of the 6 spectrometer settings are needed for each of both KIN II and III. Similarly for KIN I, 12 hours of running at each of the 6 spectrometer settings for both the forward and backward angles will be used. A full summary of the estimated total counts for each kinematic point (summing contributions from all 6 proton settings for that point), are given in Tables 2-3. The distribution in ΔW bins is given, as is the fraction of the total ηp decay cone which we will accept for each bin. Note that the count rates quoted for KIN I(f) have already accounted for the fact that cuts on both ω and q need to be made on that forward angle data in order to provide the good ω-q phase-space overlap required for the Rosenbluth separation.

TABLE 2. Estimated p(e,e′p)η Count-Rates for KIN I

12 hours for each of 6 Proton Settings = 72 hours per KIN Luminosity = 1.1×10^{38} s^{-1}cm^{-2}					**Extraction Uncertainties** [*Assume*: ± 1% *error on cross–sections*]			
ΔW-Range	**KIN I(f)**		**KIN I(b)**		**if R = 0.1**		**if R = 0.2**	
(MeV)	Counts ($\times 10^3$)	$\Delta\Omega_\eta^*/4\pi$ (%)	Counts ($\times 10^3$)	$\Delta\Omega_\eta^*/4\pi$ (%)	$\Delta\sigma_T$ (%)	$\Delta\sigma_L$ (%)	$\Delta\sigma_T$ (%)	$\Delta\sigma_L$ (%)
0.0 - 0.8	11.1	100	14.9	100	2.2	31	2.4	17
0.8 - 1.6	19.5	100	26.0	100				
1.6 - 2.4	24.2	93	32.0	89				
2.4 - 3.2	27.1	78	35.4	73				
3.2 - 4.0	28.3	59	36.5	55				

Figure 5 shows an example of how the events are distributed in θ_η^* as a function of ΔW. From this figure, it can be seen that as ΔW increases above a few MeV, our setup begins to miss η's symmetrically about 90°. For ΔW ≃ 15 MeV in the kinematics shown (KIN II), approximately 50% of the produced η's are missed. Although we will accept events with ΔW much larger than this, analysis of these events becomes increasingly ambiguous because of the larger and larger extrapolation required to the un-measured angular regions. However, the higher ΔW events may prove useful if the dependence (as measured in the lower ΔW region) of the angular distributions on ΔW is not strong.

The statistical precision which we will obtain for these angular distributions is very high (with tens of thousands of counts in the first few MeV above threshold). Such precision will allow measurement of very small σ_{LT} and σ_{TT} components. Their contributions will be evident in our angular distributions even if their magnitude is only a few percent of the total cross section.

Finally, note that Table 2 indicates values for the expected uncertainties in extracting σ_L and σ_T for the $Q^2 = 0.65$ (GeV/c)^2 point. Although each ΔW-bin is expected to contain greater than 10^5 counts (i.e. relative statistical error < 1%) the calculated uncertainties for the extraction of the response functions assume an additional relative normalization uncertainty of ±1% for both the forward and backward cross sections. As mentioned in Section 2 above, existing data indicate that the ratio $R = \sigma_L/\sigma_T$ may lie anywhere from 0.0 to 0.4. Therefore, the uncertainties in Table 2 are calculated for R = 0.1 and 0.2. These uncertainties show that we will be able to determine R to within an absolute of approximately ± 0.03. The dominant factor in the systematic uncertainty for extracting the L and T response functions in the rapid variation in σ_v as a function of ΔW. Since (as discussed in Section 5.2) we can determine the absolute scale of ΔW to a level

TABLE 3. Estimated p(e,e′p)η Count-Rates for KIN II and KIN III

25 hours for each of 6 Proton Settings = 150 hours per KIN Luminosity = $1.1 \times 10^{38}\ s^{-1}\ cm^{-2}$					
KIN II			**KIN III**		
ΔW-Range (MeV)	Counts ($\times 10^3$)	$\Delta\Omega_\eta^*/4\pi$ (%)	ΔW-Range (MeV)	Counts ($\times 10^3$)	$\Delta\Omega_\eta^*/4\pi$ (%)
0 - 1	7.2	100	0.0 - 1.6	6.0	100
1 - 2	12.5	100	1.6 - 3.2	10.1	100
2 - 3	15.6	100	3.2 - 4.8	12.5	100
3 - 4	17.9	99	4.8 - 6.4	14.5	100
4 - 5	19.6	95	6.4 - 8.0	15.7	100
5 - 6	21.1	91	8.0 - 9.6	16.8	98
6 - 7	22.2	86	9.6 - 11.2	17.6	93
7 - 8	23.1	81	11.2 - 12.8	18.5	86
8 - 9	24.0	76	12.8 - 14.4	18.5	78
9 - 10	24.5	71	14.4 - 16.0	18.5	68
10 - 11	25.2	68	16.0 - 17.6	18.7	59
11 - 12	25.5	65	17.6 - 19.2	17.9	51
12 - 13	25.7	60	19.2 - 20.8	17.5	43
13 - 14	26.0	56	20.8 - 22.4	17.0	38
14 - 15	25.3	50	22.4 - 24.0	16.5	33

of 0.1 MeV, the relative systematic uncertainty introduced into the forward and backward cross sections by our knowledge of ΔW is in the range of 1-2%. Contributions to the systematic uncertainty in these cross sections from other variations (i.e. photon flux factor, epsilon, etc.) are small compared to this variation. Thus, the systematic uncertainty in our extraction of all of the response functions (L, T, and LT and TT) enters at approximately the same level as our knowledge of relative normalization of the cross sections (±1%).

5.4 Backgrounds

Singles rates for (e,e′) and (e,p) were calculated using the computer codes QFS and EPC [Lig 88]. Figure 6 shows typical (e,e′) and (e,p) cross sections for our kinematics KIN I(f), where the proton singles-rate is highest. From these rates, accidental (e,e′p) rates were calculated assuming a 1 ns timing resolution. Since our "true" p(e,e′p)η events will populate only a very particular and small part of the accepted kinematical

phase-space (e.g. M_{miss} 547.45 ± 1.0-3.0 MeV, and $\Delta W \lesssim 20$ MeV), only a small fraction of any accidental (e,e′p) events will fall in our "coincidence" region of interest. Therefore, to properly estimate the accidental background, only those accidental events populating these regions of interest are included. Sample distributions of the accidental events in both M_{miss} and W are shown in Figure 6. Tables 4-7 contain all the specific values for the singles rates and the accidental yields, along with the calculated Signal to Noise ratios for the coincidence regions of interest. For the higher Q^2 points, contributions from accidental (e,e′p) events is negligible (S/N $\gtrsim$ 1000). At $Q^2 = 0.65$ (GeV/c)^2, the accidental background is also small, contributing at the level of S/N = 17-75.

TABLE 4. Count-rate estimates for **KIN I(f)**

$Q^2_{central} = 0.65$ (GeV/c)^2; Forward e$^-$ Angle ($E_o = 4$ GeV) $\Delta\phi_e^{transport} = \pm 10$ mr, $\Delta\theta_e^{transport} = \pm 10$ mr								
Luminosity = 1.1×10^{38} s^{-1} cm^{-2} * *Coinc.Region* ≡ (M_{miss} = 547.7 ± 2.0 MeV) & (*W = 1487.7 ± 2.0 MeV*)								
	TRUES	**SINGLES**					**S/N**	**TIME**
Proton Setting	$Y^{true}_{e,e'p\eta}$ (hr^{-1})	$Y_{e,e}$ (kHz)	Y_{e,π^-} (kHz)	$Y_{e,p}$ (kHz)	Y_{e,π^+} (kHz)	$Y^{acc}_{e,e'p}$ (hr^{-1}) [in Coinc.Region]*		(hr)
1	1228	10.9	0.8	219.6	432.2	60	20	12
2	6133			199.6	330.6	147	41	12
3	1012			173.2	244.7	42	24	12
4	8084			209.5	346.2	48	28	12
5	5960			234.6	450.0	168	35	12
6	1146			251.7	567.7	69	17	12

TABLE 5. Count-rate estimates for **KIN I(b)**

$Q^2_{central} = 0.65$ (GeV/c)^2; Backward e^- Angle ($E_o = 1.6$ GeV) $\Delta\phi_e^{transport} = \pm 30$ mr, $\Delta\theta_e^{transport} = \pm 60$ mr								
Luminosity = 1.1×10^{38} s^{-1} cm^{-2} * *Coinc.Region* ≡ ($M_{miss} = 547.7 \pm 2.0$ MeV) & ($W = 1487.7 \pm 2.0$ MeV)								
	TRUES	**SINGLES**					**S/N**	**TIME**
Proton Setting	$Y^{true}_{e,e'p\eta}$ (hr^{-1})	$Y_{e,e}$ (kHz)	Y_{e,π^-} (kHz)	$Y_{e,p}$ (kHz)	Y_{e,π^+} (kHz)	$Y^{acc}_{e,e'p}$ (hr^{-1}) [in Coinc.Region]*		(hr)
1	839	2.7	73.8	134.6	381.7	25	33	12
2	4741			120.5	293.1	64	74	12
3	699			103.0	214.3	19	37	12
4	952			121.1	305.8	20	48	12
5	4204			138.3	400.0	70	60	12
6	632			151.3	500.8	25	25	12

TABLE 6. Count-rate estimates for **KIN II**

$Q^2_{central} = 3.0$ (GeV/c)^2; $E_o = 4.0$ GeV $\Delta\phi_e^{transport} = \pm 30$ mr, $\Delta\theta_e^{transport} = \pm 60$ mr								
Luminosity = 1.1×10^{38} s^{-1} cm^{-2} * *Coinc.Region* ≡ ($M_{miss} = 547.7 \pm 2.0$ MeV) & ($W = 1493.2 \pm 7.5$ MeV)								
	TRUES	**SINGLES**					**S/N**	**TIME**
Proton Setting	$Y^{true}_{e,e'p\eta}$ (hr^{-1})	$Y_{e,e}$ (kHz)	Y_{e,π^-} (kHz)	$Y_{e,p}$ (kHz)	Y_{e,π^+} (kHz)	$Y^{acc}_{e,e'p}$ (hr^{-1}) [in Coinc.Region]*		(hr)
1	1518	0.46	1.3	66.4	76.4	1.4	1080	25
2	3549			42.2	43.7	1.4	2530	25
3	1231			24.7	22.9	0.5	2460	25
4	1663			43.8	55.0	0.8	2080	25
5	3392			68.1	94.2	2.1	1610	25
6	1285			99.3	150.6	1.8	710	25

TABLE 7. Count-rate estimates for **KIN III**

$Q^2_{central} = 4.0$ (GeV/c)^2; $E_o = 6.0$ GeV $\Delta\phi_e^{transport} = \pm 30$ mr, $\Delta\theta_e^{transport} = \pm 30$ mr								
Luminosity = 1.1×10^{38} s^{-1}cm^{-2} * *Coinc.Region* ≡ ($M_{miss} = 547.7 \pm 2.0$ MeV) & ($W = 1497.7 \pm 12$ *MeV*)								
	TRUES	**SINGLES**					**S/N**	**TIME**
Proton Setting	$Y^{true}_{e,e'p\eta}$ (hr^{-1})	$Y_{e,e}$ (kHz)	Y_{e,π^-} (kHz)	$Y_{e,p}$ (kHz)	Y_{e,π^+} (kHz)	$Y^{acc}_{e,e'p}$ (hr^{-1}) [in Coinc.Region]*		(hr)
1	1388	0.48	0.08	37.2	32.1	0.7	1980	25
2	2380			20.4	16.0	0.5	4760	25
3	1050			10.0	7.1	0.2	5250	25
4	1334			21.6	20.9	0.3	4440	25
5	2137			38.9	41.0	0.8	2670	25
6	1166			64.2	73.4	1.0	1160	25

Also given in Tables 4-7, and shown in Figure 6, are the contributions from singles π^- and π^+ background. These were also calculated with the EPC code, which has a parameterization of multiple-pion production included. The π^- to electron ratio is generally quite favourable, except at the backward KIN I(b) where the ratio is ≈ 30. The π^+ to proton ratio gets only as high as ≈ 3. Again, due to the narrow phase space of our coincidence region of interest, even a pion rejection ratio of 1% would suffice to avoid any significant contributions from pion contamination (design goal rejection ratio is 10^{-6}). Note that the total singles rate of both π^+ and protons can become relatively high, particularly for KIN I(f) where the rate can reach about 820 kHz; this rate should still be acceptable, with the VDC's designed to handle singles rates up to 1 MHz.

Finally note that, as has been true for all previous p(e,e′p)η experiments, there will be unavoidable background present from those p(e,e′p)ππ events which populate the coincidence region of interest. However, because of our unprecedented missing mass resolution for this type of experiment, the contribution from these events will be minimized. We expect this background to be at the level of 10% or less of our true rate.

5.5 Summary

We propose to measure the full center-of-mass η angular distributions from the p(e,e′p)η reaction in the region near threshold for Q^2 = 4.0, 3.0, and 0.65 $(GeV/c)^2$. The angular distributions will be mapped as a function of excitation energy with very good resolution in both energy ($\delta W \simeq 1.0$ MeV FWHM) and angle ($\delta\theta_\eta^* < 5°$ FWHM, $\delta\phi_\eta <$ 10° FWHM). We will obtain sufficient statistical and systematic precision to allow measurements of the σ_{LT} and σ_{TT} interference terms even if they are as small as a few percent of the total cross section. In addition, a Rosenbluth separation will be done at the lowest Q^2 value, allowing extraction of the ratio $R = \sigma_L/\sigma_T$ to a level of $\pm$ 0.03.

6. Summary of Beam Time Requested

Below is a summary of the requested to perform the measurements proposed. All times assume the previously quoted luminosity of 1.1×10^{38} $s^{-1}cm^{-2}$.

BEAM TIME:

KIN I(f)	$Q^2 = 0.65$ $(GeV/c)^2$	$E_o = 4.0$ GeV	6×12 hours	→	72 hours
KIN I(b)	$Q^2 = 0.65$ $(GeV/c)^2$	$E_o = 1.6$ GeV	6×12 hours	→	72 hours
KIN II	$Q^2 = 3.0$ $(GeV/c)^2$	$E_o = 4.0$ GeV	6×25 hours	→	150 hours
KIN III	$Q^2 = 4.0$ $(GeV/c)^2$	$E_o = 6.0$ GeV	6×25 hours	→	150 hours
			TOTAL	→	444 hours

OVERHEAD TIME

Target cool-down and setup	→	12 hours
Spectrometer diagnostics	→	48 hours
Angle and momentum changes	→	24 hours
GRAND TOTAL	→	**528 hours**

REFERENCES

Ald 75 — J.-C. Alder *et al.*, Nuc. Phys. **B91**, 386 (1975).

Baj 69 — R.P. Bajpai and A. Donnachie, Nuc. Phys. **B12**, 274 (1969).

Ben 94 — M. Benmerrouch, N.C. Mukhopadhyay, and J.F. Zhang, *Effective Lagrangian Approach to the Theory of Eta Photoproduction in the N^* (1535) Region*, LANL Preprint HEP-PH/9412248.

Bra 78 — F.W. Brasse *et al.*, Nuc. Phys. **B139** 37 (1978).

Bra 84 — F.W. Brasse *et al.*, Z. Phys. **C22** 33 (1984).

Bre 78 — H. Breuker *et al.*, Phys. Lett. **74B**, 409 (1978).

CDR 90 — CEBAF *Conceptual Design Report: Basic Experimental Equipment* (revised), April 1990.

CLAS 89 — CLAS Experiment Proposal, S. Dytman *et al.*, *A Study of the $S_{11}(1535)$ and $P_{11}(1710)$ in $p(e,e'p)\eta$*, CEBAF PR-89-039 (1989).

Dom 69 — N. Dombey, Rev. Mod. Phys. **41**, 236 (1969).

Dor 90 — A.E. Dorokhov, N.I. Koshelev, in *High Energy Spin Physics, Proc. of the 9th International Symposium*, Bonn, FRG, Sept. 6-15 (1990), Springer-Verlag, p. 444; N.A. Tornquist, *ibid.*, p. 432; A.V. Efremov, *ibid.*, p. 430.

Efr 90 — A.V. Efremov, J. Soffer, N.A. Tornquist, Phys. Rev. Lett. **64**, 1495 (1990).

Fos 83 — F. Foster and G. Hughes, Rep. Prog. Phys. **46**, 1445 (1983).

Got 94 — R. Gothe, private communication.

Hat 90 — T. Hatsude, Nucl. Phys. **B329**, 376 (1990).

Kon 80 — R. Koniuk and N. Isgur, Phys. Rev. **D21**, 1868 (1980).

Kon 90 — W. Konen and H.J. Weber, Phys. Rev. **D41**, 2201 (1990).

Kum 73 — P.S. Kummer *et al.*, Phys. Rev. Lett. **30**, 873 (1973).

Lig 88 — J. Lightbody and J. O'Connell, Computers in Physics **2**, 57 (1988).

Par 94 — Particle Data Group, Phys. Rev. **D50**, 1173 (1994).

Ras 89 — A.S. Raskin and T.W. Donnelly, Annals of Phys. **191**, 78 (1989).

TAPS 94	TAPS Collaboration (B. Krusche *et al.*); these results have been presented by B. Krusche at recent conferences: Dubna (1994), Trieste (1993), and Perugia (1993).
Tia 94	L. Tiator, C. Bennhold, and S.S. Kamalov, Mainz preprint, No. MKPH-T-94-3 (1994).
Ulm 91	P.E. Ulmer, *MCEEP: Monte Carlo for Electro-Nuclear Coincidence Experiments*, CEBAF Technical Note 91-101 (1991).
Wil 93	M. Wilhelm, Ph.D. thesis, Bonn (1993).

FIGURE CAPTIONS

Figure 1 Total cross section data for $\gamma_v p \rightarrow S_{11}(1525)$ and for $\gamma_v p \rightarrow D_{13}(1520)$, as presented in [Bra 84].

Figure 2 Kinematic contours for $p(e,e'p)\eta$ at threshold (ΔW = 0 MeV). The solid lines are contours for E_o fixed at 1.6, 4.0, and 6.0 GeV, and the dashed lines for Q^2 fixed at 0.05, 0.20, and 0.65 $(GeV/c)^2$.

Figure 3 Example of "kinematic focusing" effect. With electron kinematics fixed at the central values for KIN II, shown in the space of (Proton lab momentum) vs. (Proton angle with respect to $\vec{q}$) are lines of constant ΔW (solid lines) and θ_η^* (dashed lines).

Figure 4 Kinematic phase-space coverage for KIN II for $p(e,e'p)\eta$ with ΔW = 0-15 MeV. The top graph shows the population of the scattered electron momentum and angle, along with the limits of the spectrometer acceptances shown by the solid lines. The bottom two graphs show the population in the proton spectrometer coordinates. The central proton coordinates $(\phi_p^{transport}, \theta_p^{transport}) = (0°, 0°)$ are defined along the central $\vec{q}$ direction (θ_q = -21.46°). The solid indicate the limits of spectrometer acceptances for each of the 6 proton settings.

Figure 5 Variation of estimated total counts and acceptances for $p(e,e'p)\eta$ as a function of $\cos(\theta_\eta^*)$ for various ΔW ranges. Results are shown for the sum of all 6 proton spectrometer-settings for KIN II after 150 hours running (25 hours per setting).

Figure 6 Accidental rates and singles cross sections for KIN I(f), proton setting #1. The top 2 graphs show how the accidental (e,e'p) yield populate missing mass and W; the dashed lines indicate the coincidence regions of interest for the $p(e,e'p)\eta$ data. The bottom 2 graphs show the individual (e,e'), (e,p), (e,π^-), and (e,π^+) cross sections which contribute.

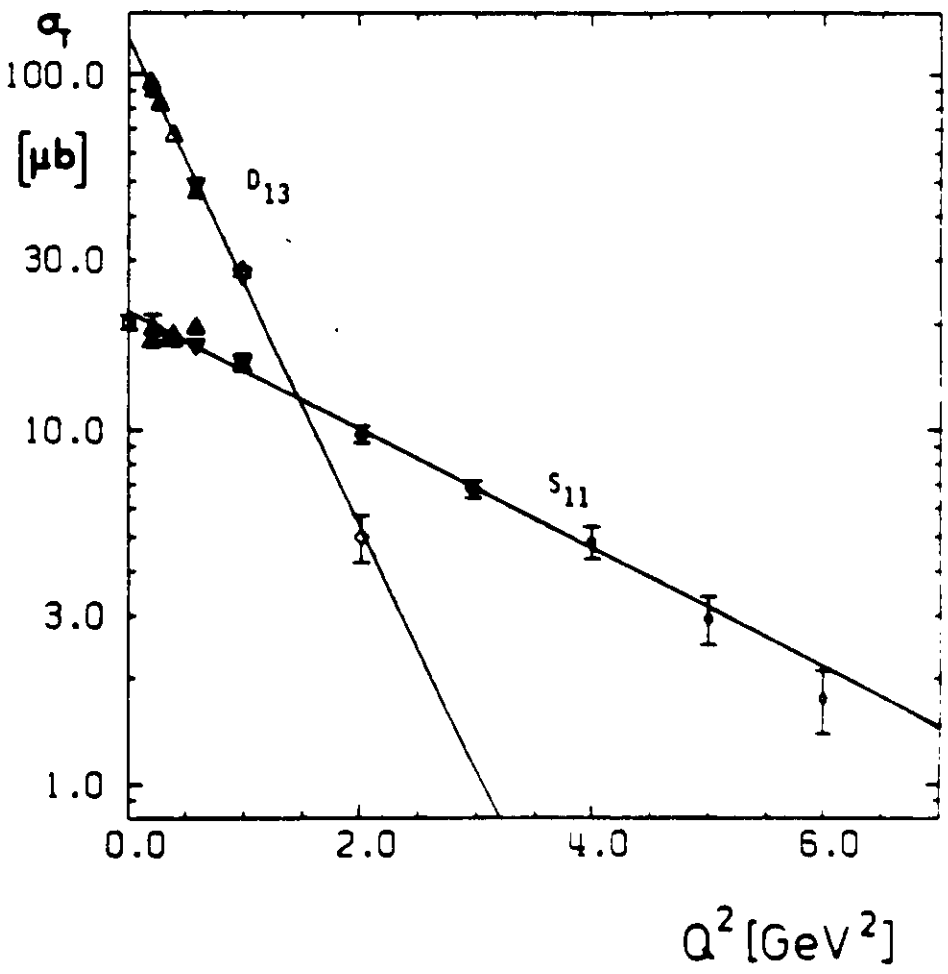

FIGURE 1

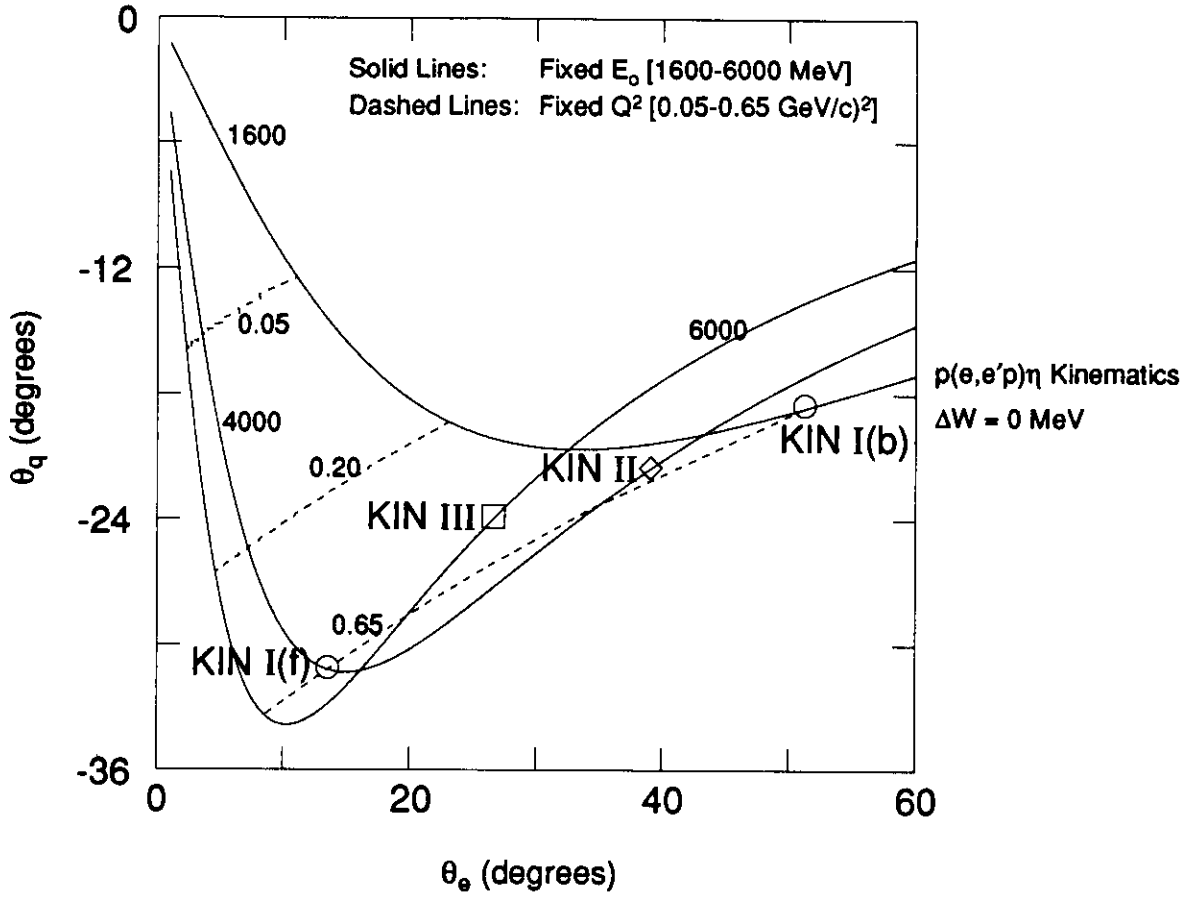

FIGURE 2

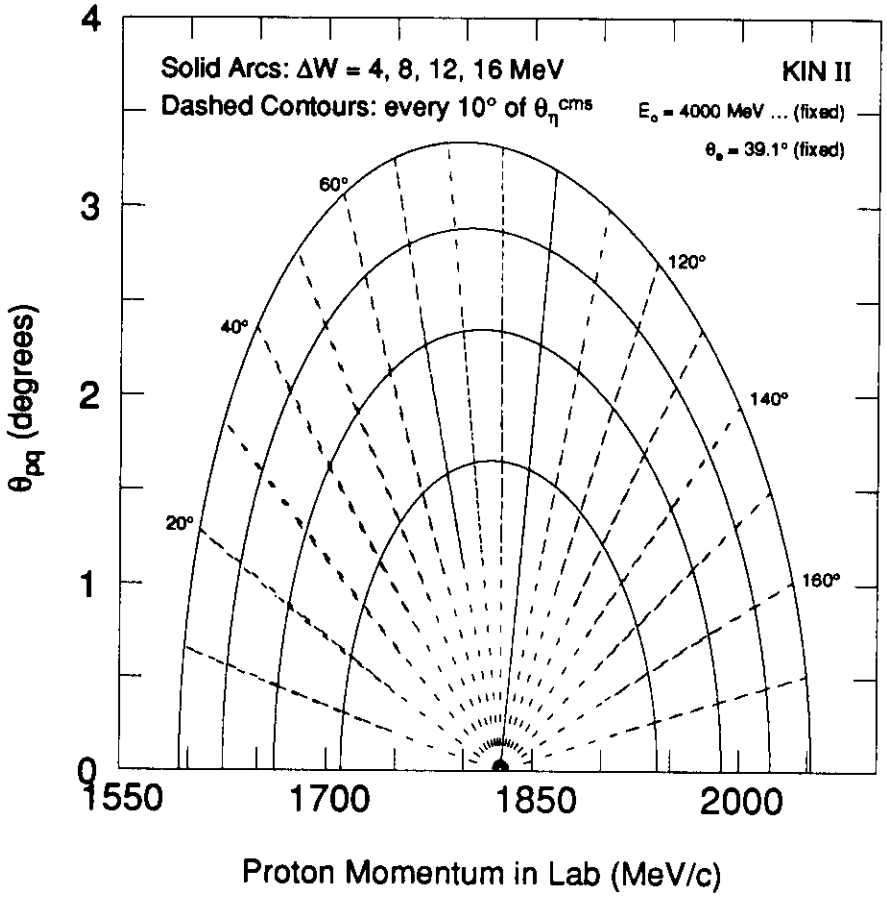

FIGURE 3

p(e,e'p)η Kinematics: KIN II

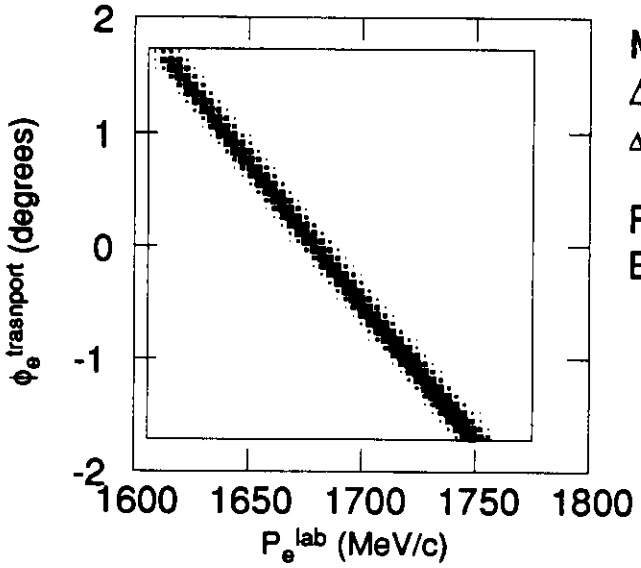

Monte Carlo Results:
$\Delta W = 0.00 \rightarrow 15.0$ MeV
$\Delta W_{central} = 7.50$ MeV

FULL
ELECTRON ACCEPTANCE.
$\Delta\phi_e^{transport} = \pm 30$ mr
$\Delta\theta_e^{transport} = \pm 60$ mr

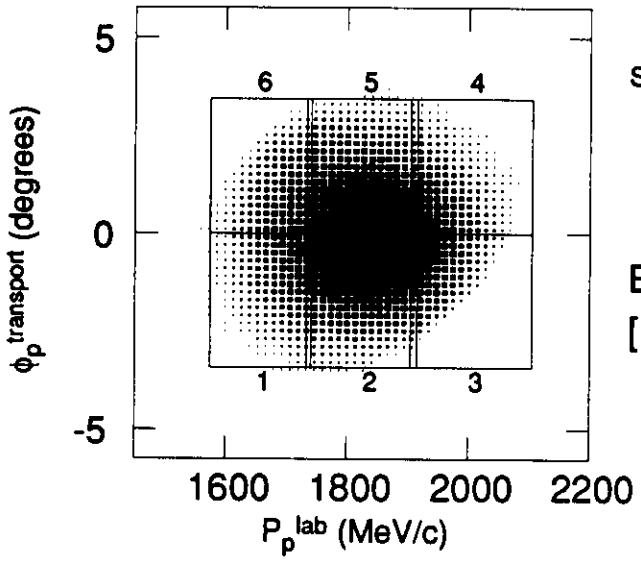

Sampling: Weighted by S11 Cross section

$E_o = 4000$ MeV
[$Q^2 = 3.00$ (GeV/c)^2]

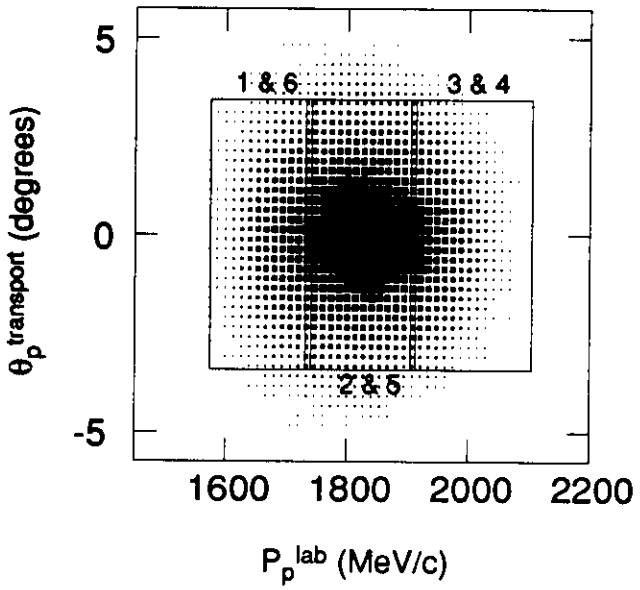

FIGURE 4

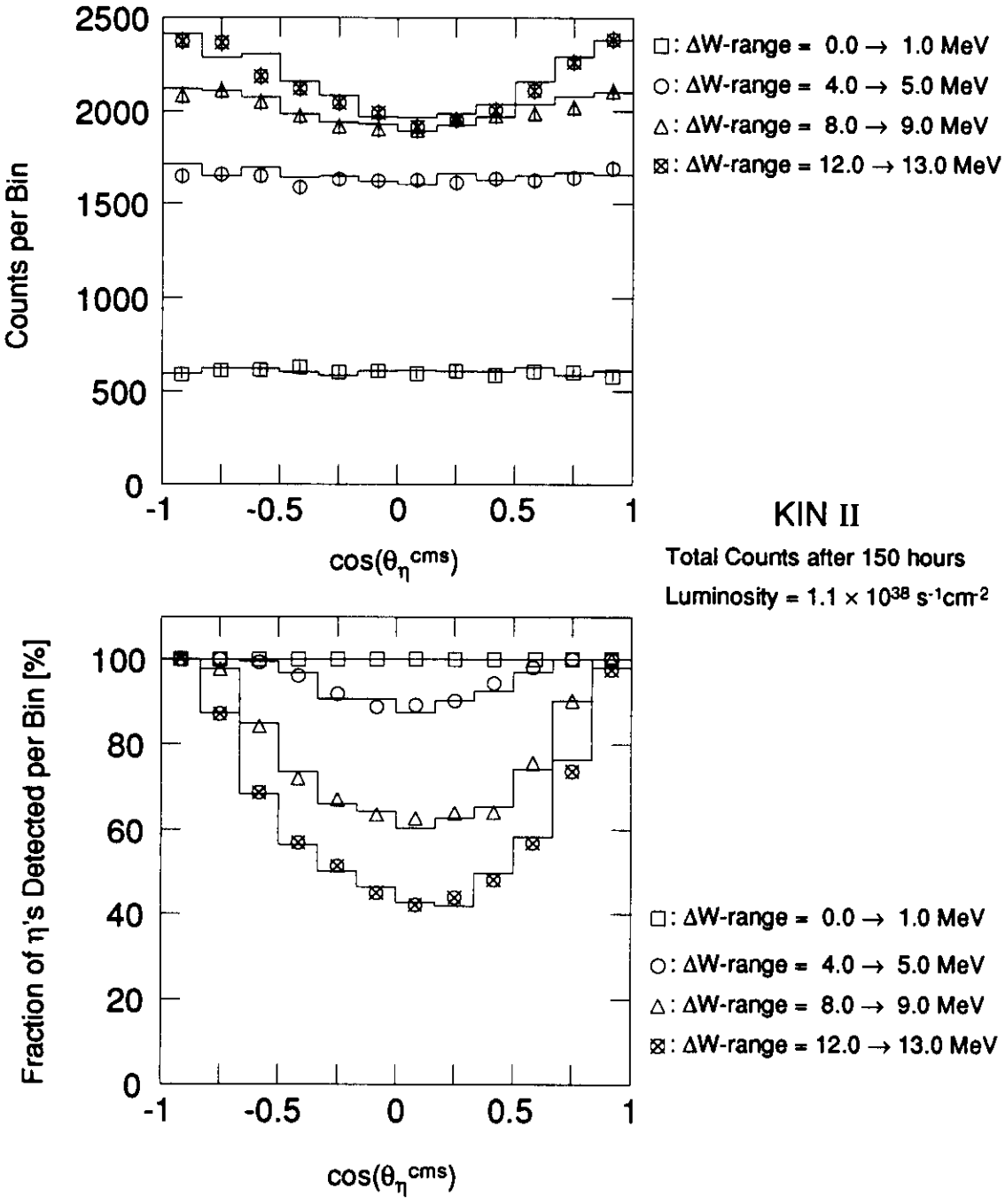
Counts per Bin
2500
2000
1500
1000
500
0
-1
-0.5
0
0.5
1
cos(θη cms)
□: ΔW-range = 0.0 → 1.0 MeV
○: ΔW-range = 4.0 → 5.0 MeV
△: ΔW-range = 8.0 → 9.0 MeV
⊠: ΔW-range = 12.0 → 13.0 MeV
KIN II
Total Counts after 150 hours
Luminosity = 1.1 × 10^38 s^-1cm^-2
Fraction of η's Detected per Bin [%]
100
80
60
40
20
0
-1
-0.5
0
0.5
1
cos(θη cms)
□: ΔW-range = 0.0 → 1.0 MeV
○: ΔW-range = 4.0 → 5.0 MeV
△: ΔW-range = 8.0 → 9.0 MeV
⊠: ΔW-range = 12.0 → 13.0 MeV

FIGURE 5

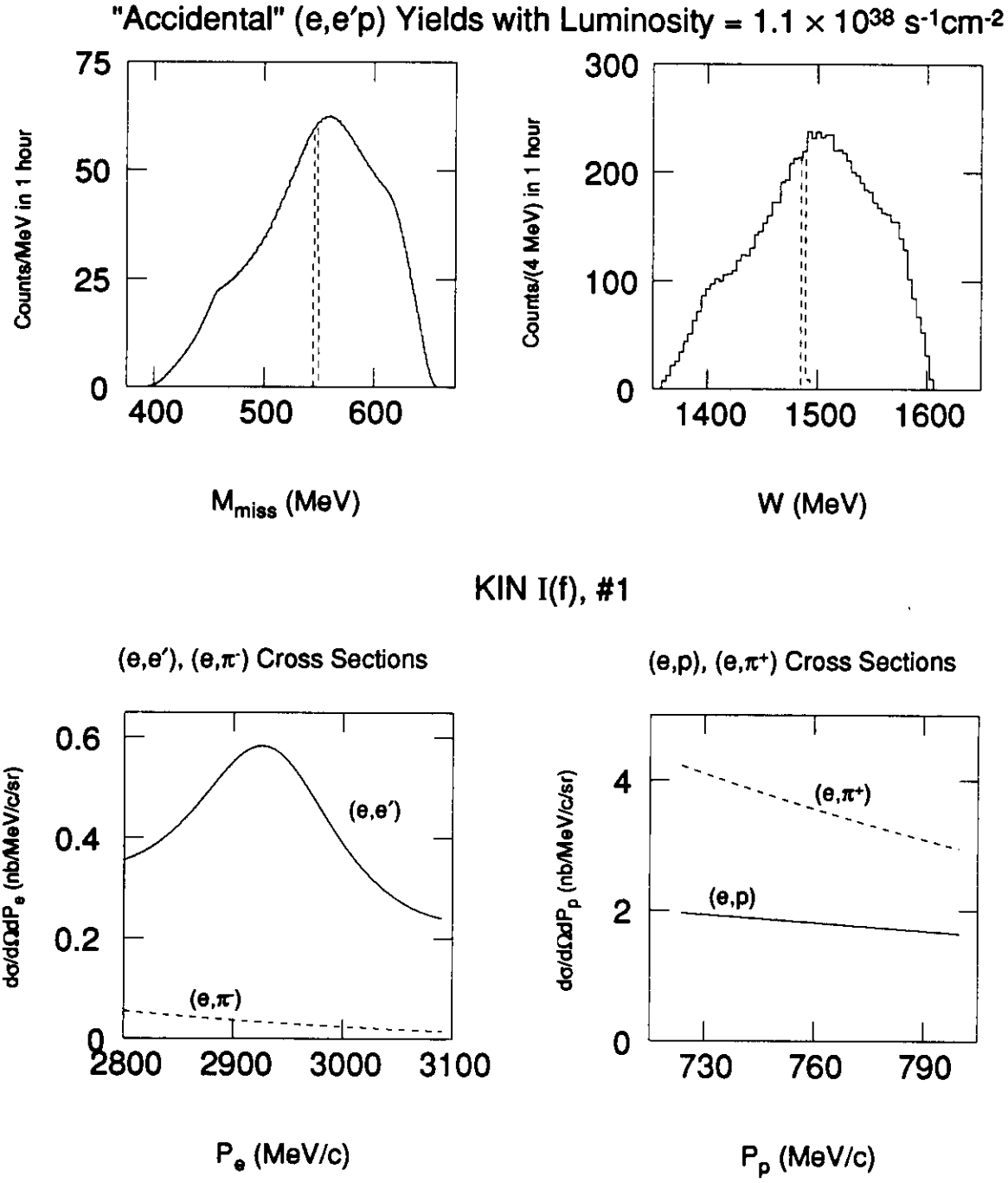
"Accidental" (e,e'p) Yields with Luminosity = 1.1 × 10^38 s^-1cm^-2
Counts/MeV in 1 hour
75
50
25
0
400
500
600
M_miss (MeV)
Counts/(4 MeV) in 1 hour
300
200
100
0
1400
1500
1600
W (MeV)
KIN I(f), #1
(e,e'), (e,π⁻) Cross Sections
dσ/dΩdP_e (nb/MeV/c/sr)
0.6
0.4
0.2
0
(e,e')
(e,π⁻)
2800
2900
3000
3100
P_e (MeV/c)
(e,p), (e,π⁺) Cross Sections
dσ/dΩdP_p (nb/MeV/c/sr)
4
2
0
(e,π⁺)
(e,p)
730
760
790
P_p (MeV/c)

FIGURE 6